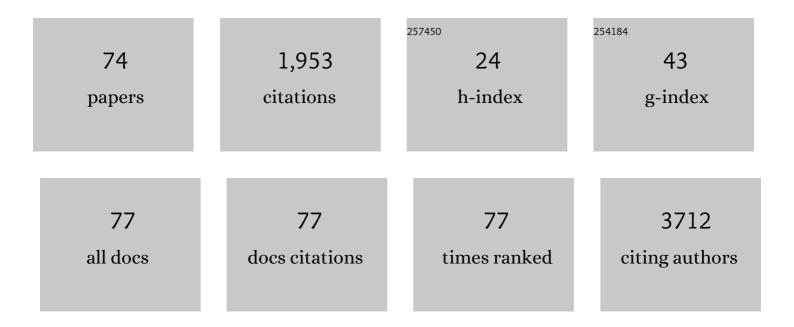
Jeffery Aguiar

List of Publications by Year in descending order

Source: https://exaly.com/author-pdf/527056/publications.pdf Version: 2024-02-01



IFFFFDY ACHIAD

#	Article	IF	CITATIONS
1	CdTe solar cells with open-circuit voltage breaking the 1 V barrier. Nature Energy, 2016, 1, .	39.5	307
2	A graded catalytic–protective layer for an efficient and stable water-splitting photocathode. Nature Energy, 2017, 2, .	39.5	135
3	Atomic-Scale Imaging and Spectroscopy for <i>In Situ</i> Liquid Scanning Transmission Electron Microscopy. Microscopy and Microanalysis, 2012, 18, 621-627.	0.4	125
4	Decoding crystallography from high-resolution electron imaging and diffraction datasets with deep learning. Science Advances, 2019, 5, eaaw1949.	10.3	81
5	Oxidatively Stable Nanoporous Silicon Photocathodes with Enhanced Onset Voltage for Photoelectrochemical Proton Reduction. Nano Letters, 2015, 15, 2517-2525.	9.1	80
6	In situ investigation of the formation and metastability of formamidinium lead tri-iodide perovskite solar cells. Energy and Environmental Science, 2016, 9, 2372-2382.	30.8	79
7	Interfacial Ferromagnetism in <mml:math <br="" xmlns:mml="http://www.w3.org/1998/Math/MathML">display="inline"><mml:msub><mml:mi>LaNiO</mml:mi><mml:mn>3</mml:mn></mml:msub><mml:mo>/Physical Review Letters, 2013, 111, 087202.</mml:mo></mml:math>	:m ø. 8< mm	ıl:m s ub> <m< td=""></m<>
8	Black carbon concentrations and diesel vehicle emission factors derived from coefficient of haze measurements in California: 1967–2003. Atmospheric Environment, 2008, 42, 480-491.	4.1	64
9	Effect of helium irradiation on Ti3AlC2 at 500°C. Scripta Materialia, 2014, 77, 1-4.	5.2	51
10	Thermal Expansion, Heat Capacity, and Thermal Conductivity of Nickel Ferrite (NiFe ₂ O ₄). Journal of the American Ceramic Society, 2014, 97, 1559-1565.	3.8	51
11	Sodium Accumulation at Potential-Induced Degradation Shunted Areas in Polycrystalline Silicon Modules. IEEE Journal of Photovoltaics, 2016, 6, 1440-1445.	2.5	48
12	Unbiased solar H ₂ production with current density up to 23 mA cm ^{â^'2} by Swiss-cheese black Si coupled with wastewater bioanode. Energy and Environmental Science, 2019, 12, 1088-1099.	30.8	48
13	Termination chemistry-driven dislocation structure at SrTiO3/MgO heterointerfaces. Nature Communications, 2014, 5, 5043.	12.8	39
14	Bubble formation and lattice parameter changes resulting from He irradiation of defect-fluorite Gd2Zr2O7. Acta Materialia, 2016, 115, 115-122.	7.9	39
15	Thermodynamics versus kinetics of grain growth control in nanocrystalline zirconia. Acta Materialia, 2017, 136, 224-234.	7.9	38
16	Low-cost plasma immersion ion implantation doping for Interdigitated back passivated contact (IBPC) solar cells. Solar Energy Materials and Solar Cells, 2016, 158, 68-76.	6.2	37
17	SANS and TEM of ferritic–martensitic steel T91 irradiated in FFTF up to 184dpa at 413°C. Journal of Nuclear Materials, 2013, 440, 91-97.	2.7	36
18	Interface Energies of Nanocrystalline Doped Ceria: Effects of Manganese Segregation. Journal of Physical Chemistry C, 2015, 119, 27855-27864.	3.1	36

JEFFERY AGUIAR

#	Article	IF	CITATIONS
19	Electrophobic interaction induced impurity clustering in metals. Acta Materialia, 2016, 119, 1-8.	7.9	36
20	Structure and segregation of dopant–defect complexes at grain boundaries in nanocrystalline doped ceria. Physical Chemistry Chemical Physics, 2015, 17, 15375-15385.	2.8	33
21	Localized corrosion of low-carbon steel at the nanoscale. Npj Materials Degradation, 2019, 3, .	5.8	31
22	Effect of Water Vapor, Temperature, and Rapid Annealing on Formamidinium Lead Triiodide Perovskite Crystallization. ACS Energy Letters, 2016, 1, 155-161.	17.4	27
23	Crystallographic prediction from diffraction and chemistry data for higher throughput classification using machine learning. Computational Materials Science, 2020, 173, 109409.	3.0	27
24	Linking Interfacial Step Structure and Chemistry with Locally Enhanced Radiationâ€Induced Amorphization at Oxide Heterointerfaces. Advanced Materials Interfaces, 2014, 1, 1300142.	3.7	25
25	Probing battery chemistry with liquid cell electron energy loss spectroscopy. Chemical Communications, 2015, 51, 16377-16380.	4.1	25
26	Revealing Surface Modifications of Potassiumâ€Fluorideâ€Treated Cu(In,Ga)Se ₂ : A Study of Material Structure, Chemistry, and Photovoltaic Performance. Advanced Materials Interfaces, 2016, 3, 1600013.	3.7	24
27	Solar wind contributions to Earthâ \in ^M s oceans. Nature Astronomy, 2021, 5, 1275-1285.	10.1	22
28	Defect interactions with stepped CeO2/SrTiO3 interfaces: Implications for radiation damage evolution and fast ion conduction. Journal of Chemical Physics, 2014, 140, 194701.	3.0	21
29	Non-uniform Solute Segregation at Semi-Coherent Metal/Oxide Interfaces. Scientific Reports, 2015, 5, 13086.	3.3	21
30	Bringing nuclear materials discovery and qualification into the 21st century. Nature Communications, 2020, 11, 2556.	12.8	18
31	Combined effects of radiation damage and He accumulation on bubble nucleation in Gd2Ti2O7. Journal of Nuclear Materials, 2016, 479, 542-547.	2.7	16
32	Revealing the semiconductor–catalyst interface in buried platinum black silicon photocathodes. Journal of Materials Chemistry A, 2016, 4, 8123-8129.	10.3	15
33	Orientation-specific amorphization and intercalated recrystallization at ion-irradiated SrTiO ₃ /MgO interfaces. Journal of Materials Research, 2014, 29, 1699-1710.	2.6	14
34	Mapping strain modulated electronic structure perturbations in mixed phase bismuth ferrite thin films. Journal of Materials Chemistry C, 2015, 3, 1835-1845.	5.5	14
35	Quantifying the low-energy limit and spectral resolution in valence electron energy loss spectroscopy. Ultramicroscopy, 2013, 124, 130-138.	1.9	13
36	Contrasting the Material Chemistry of Cu ₂ ZnSnSe ₄ and Cu ₂ ZnSnS _{(4–} <i>_x</i> ₎ Se <i>_x</i> Advanced Science, 2016, 3, 1500320.	11.2	13

JEFFERY AGUIAR

#	Article	IF	CITATIONS
37	Dual Protection Layer Strategy to Increase Photoelectrode–Catalyst Interfacial Stability: A Case Study on Black Silicon Photoelectrodes. Advanced Materials Interfaces, 2019, 6, 1802085.	3.7	13
38	Advances in the electron diffraction characterization of atomic clusters and nanoparticles. Nanoscale Advances, 2021, 3, 311-325.	4.6	13
39	Hidden one-dimensional spin modulation in a three-dimensional metal. Nature Communications, 2014, 5, 4218.	12.8	12
40	Studying Perovskite-based Solar Cells with Correlative In-Situ Microscopy. Microscopy and Microanalysis, 2015, 21, 969-970.	0.4	11
41	Cation ratio fluctuations in Cu ₂ ZnSnS ₄ at the 20 nm length scale investigated by analytical electron microscopy. Physica Status Solidi (A) Applications and Materials Science, 2016, 213, 2392-2399.	1.8	11
42	Role of the interface on radiation damage in the SrTiO3/LaAlO3 heterostructure under Ne2+ ion irradiation. Journal of Applied Physics, 2014, 115, .	2.5	10
43	Interface Characterization of Single-Crystal CdTe Solar Cells With VOC > 950 mV. IEEE Journal of Photovoltaics, 2016, 6, 1650-1653.	2.5	10
44	Solute redistribution and phase stability at FeCr/TiO2â^' interfaces under ion irradiation. Acta Materialia, 2015, 89, 364-373.	7.9	9
45	Irradiation-induced formation of a spinel phase at the FeCr/MgO interface. Acta Materialia, 2015, 93, 87-94.	7.9	8
46	A Strategy to Mitigate Grain Boundary Blocking in Nanocrystalline Zirconia. Journal of Physical Chemistry C, 2018, 122, 26344-26352.	3.1	8
47	Module degradation mechanisms studied by a multi-scale approach. , 2016, , .		7
48	In situ investigation of halide incorporation into perovskite solar cells. MRS Communications, 2017, 7, 575-582.	1.8	7
49	Waterâ€Assisted Liftoff of Polycrystalline CdS/CdTe Thin Films Using Heterogeneous Interfacial Engineering. Advanced Materials Interfaces, 2019, 6, 1900300.	3.7	7
50	Integrating atomistic simulations and machine learning to design multi-principal element alloys with superior elastic modulus. Journal of Materials Research, 2022, 37, 1497-1512.	2.6	7
51	Cr incorporated phase transformation in Y2O3 under ion irradiation. Scientific Reports, 2017, 7, 40148.	3.3	6
52	Cadmium Selective Etching in CdTe Solar Cells Produces Detrimental Narrow-Gap Te in Grain Boundaries. ACS Applied Energy Materials, 2020, 3, 1749-1758.	5.1	6
53	Electronic structure of oxide fuels from experiment and first principles calculations. Journal of Physics: Conference Series, 2010, 241, 012062.	0.4	5
54	Observation and Implications of Composition Inhomogeneity Along Grain Boundaries in Thin Film Polycrystalline CdTe Photovoltaic Devices. Advanced Materials Interfaces, 2019, 6, 1900152.	3.7	5

JEFFERY AGUIAR

#	Article	IF	CITATIONS
55	Structureâ€Induced Stability in Sinuous Black Silicon for Enhanced Hydrogen Evolution Reaction Performance. Advanced Functional Materials, 2021, 31, 2008888.	14.9	5
56	Characterization of secondary phases and other defects in CdZnTe. , 2010, , .		4
57	Nanoscale morphologies at alloyed and irradiated metal-oxide bilayers. Journal of Materials Science, 2015, 50, 2726-2734.	3.7	4
58	Atomic scale understanding of poly-Si/SiO <inf>2</inf> /c-Si passivated contacts: Passivation degradation due to metallization. , 2016, , .		3
59	Structure and radiation response of anion excess bixbyite Gd2Ce2O7. Physical Review Materials, 2022, 6, .	2.4	3
60	Investigating the electronic structure of fluorite-structured oxide compounds: comparison of experimental EELS with first principles calculations. Journal of Physics Condensed Matter, 2012, 24, 295503.	1.8	2
61	Structural analysis of Gd2Ce2O7. Materials Research Society Symposia Proceedings, 2015, 1743, 7.	0.1	2
62	Densification of graphite under high pressure and moderate temperature. Materials Today Communications, 2020, 22, 100821.	1.9	2
63	Plasma immersion ion implantation for interdigitated back passivated contact (IBPC) solar cells. , 2016, , .		1
64	Mapping carrier lifetime variations in polycrystalline CdTe thin films using confocal microscopy. , 2018, , .		1
65	In-situ Ion Irradiation and Recrystallization in Highly Structured Materials. Microscopy and Microanalysis, 2019, 25, 1572-1573.	0.4	1
66	Structural and Compositional Properties of Recrystallized CdS/CdTe Thin-Films Grown on Oxidized Silicon Substrates. Microscopy and Microanalysis, 2019, 25, 2166-2167.	0.4	1
67	Assessing the solid-state kinetics and behavior for uranium-free Pu-12Am–40Zr alloys at 973â€⁻K. Journal of Alloys and Compounds, 2020, 817, 152735.	5.5	1
68	High Throughput Crystal Structure Classification. Microscopy and Microanalysis, 2020, 26, 10-12.	0.4	1
69	Studying the Electronic Structure of Uranium Dioxide. Microscopy and Microanalysis, 2009, 15, 1380-1381.	0.4	Ο
70	Determining the Atomic Structure of [111] Tilt Grain Boundaries in Ceria. Microscopy and Microanalysis, 2012, 18, 386-387.	0.4	0
71	Tracking the Evolution of in-situ Radiochemistry with Transmission Electron Microscopy. Microscopy and Microanalysis, 2015, 21, 1747-1748.	0.4	0
72	Pioneering the Use of Neural Network Architectures and Feature Engineering for Real-Time Augmented Microscopy and Analysis. Microscopy and Microanalysis, 2018, 24, 514-515.	0.4	0

#	Article	IF	CITATIONS
73	Freestanding Thinâ€Films: Waterâ€Assisted Liftoff of Polycrystalline CdS/CdTe Thin Films Using Heterogeneous Interfacial Engineering (Adv. Mater. Interfaces 14/2019). Advanced Materials Interfaces, 2019, 6, 1970095.	3.7	ο
74	Merging Deep Learning, Chemistry, and Diffraction for High-Throughput Material Structure Prediction. Microscopy and Microanalysis, 2019, 25, 168-169.	0.4	0